Semiconductor physics

Study of fractality nature in VO_2 films and its influence on metal-insulator phase transition

A.A. Efremov*, B.M. Romaniuk, V.P. Melnyk, O.A. Stadnik, T.M. Sabov, O.A. Kulbachinskiy, O.V. Dubikovskiy

V. Lashkaryov Institute of Semiconductors Physics, NAS of Ukraine, 41, prosp. Nauky, 03680 Kyiv, Ukraine
**Corresponding author e-mail: dr.alef007@gmail.com*

Abstract. The mechanisms underlying the origin of fractal shape of inclusions of a new phase in VO_2 films during metal-insulator phase transition are discussed. The obtained results show that hysteresis of the temperature dependence of resistance $R(T)$ significantly depends on the film morphology and texture. Moreover, some fractal features are observed. To determine the fractal dimension D of the structural elements of the studied films from their images, different fractal analysis approaches were preliminary compared and discussed. As a result of the film image treatments, the boundaries of the structural elements were found to have fractal dimensions of 1.3 to 1.5 or higher and to correlate with the shape of $R(T)$. The fractal boundaries indicate the dominant role of elastic stress on the phase transition of films, which is confirmed by numerical modeling. Based on these results, an analytical model is proposed that relates the free energy of a film to the fractal dimension of its constituents. Depending on the ratio of the elastic and interface specific energies, the position of the free energy minimum F corresponds to a certain fractal dimensionality D. A small interface energy leads to a higher fractal dimension making the initial phase more stable. This conclusion explains well all the effects observed experimentally in VO_2. The obtained results provide a better understanding of the influence of structure and morphology on other properties of the studied films.

Keywords: metal-insulator phase transition, VO_2 films, numerical modeling.

https://doi.org/10.15407/spqeo27.01.028
PACS 62.20.de, 68.37.Ps, 68.55.Ln, 68.60.Bs, 78.30.j, 81.40.Jj

Manuscript received 26.12.23; revised version received 27.01.24; accepted for publication 28.02.24; published online 12.03.24.

1. Introduction

Traditionally, metal-insulator transition (MIT) in VO_2 films is detected by changes in such macroscopic parameters as conductivity, transparency, *etc*. At the same time, modern research methods (Kelvin probe microscopy and/or near-field infrared spectroscopy) allow a detailed visualization of the evolution of the shape of metallic inclusions in a dielectric matrix and *vice versa* [1]. The respective data show that inclusions of a new phase are fractal objects in both cases.

The fractal character of the inclusions of both phases is also well illustrated by the images obtained with a scanning near-field infrared microscope. Such images show coexistence of inclusions of metallic and insulating phases with indented (or fringed) boundaries in thin VO_2 films [2].

The questions naturally arises: Why do the structural elements in the case of MIT have fractal rather than rounded or faceted shape, what exactly does the value of the fractal dimension depend on, and what is the mechanism of the appearance of fractal objects in VO_2 films? The present work is intended to answer this question. First, we clarify the concept of fractal and fractal dimension. There are several close definitions of fractal reflecting its different aspects. Here are some of them.

Fractals are the sets with highly irregular branched or indented structure. Fractal objects are fundamentally non-smooth, fractured everywhere and having a complex structure [3].

Mandelbrot [4] gave a mathematical description of a fractal as a set, whose dimension D strictly exceeds the topological dimension. Hence, the dimension of a fractal curve is in the range $1 < D < 2$, and that of a fractal surface $2 < D_S < 3$.

Therefore, a fractal is a fractured, indented (non-smooth) object having a fractional dimension. For a surface profile or a boundary of a certain closed area, the fractal dimension, which depends on the complexity of the object (the extent to which its boundaries are rugged, irregular and winding [4]), lies in the range $1 < D < 2$. One of the ways to determine the fractal dimension of some set of bounded two-dimensional regions of different sizes is to plot the dependence of the perimeter P of such regions on their area A on a double logarithmic scale. Then the slope of the dependence $\lg P(\lg A)$ gives a value equal to half of the fractal dimension of the boundary. The same method was applied in [1] when analyzing MIT in VO_2. It turned out that for the whole ensemble of inclusions (even at different temperatures in the vicinity of MIT), D is the same and can reach the value of 1.488 [1]. We also use this method of determining the fractal dimension in the present work.

2. Methods for determining fractal dimension from image

As noted in [5], there is still practically neither a uniform consistently reproducible mathematical (and even more so algorithmic) approach to study the fractal properties, nor a generally recognized unified software.

A fairly complete overview of various methods of fractal analysis is presented in the Gwyddion software manual [6]. These methods are implemented in the software itself. In particular, they include the cube counting method [7, 8], the triangulation method [7], the variational method [9, 10], and the power spectrum method [9–11].

At the same time, the software [6] does not comprise an implemented method of determining the fractal dimension D based on the analysis of the relation between the perimeters and the areas, which was discussed above. The Gwyddion software finds the fractal dimension of the surface D_S, which is one unit greater than the dimension of the contour line D, encircling a flat fractal object, $D = D_S - 1$ [4]. All the results and calculations presented below in this paper, refer to the fractal dimension of boundaries D. The tests demonstrated that Gwyddion performs well for some classical fractals such as the "British Coastline" [3, 4] ($D = 1.21$). However, for ordinary ($D = 1$) and complex Euclidean shapes ($D = 1.001$) as well as for fractals with high dimensions ($D > 1.5$) it gives noticeable errors, overestimating D by several tenths in the first case and underestimating it in the second case.

For this reason, we have created a software to calculate the value of D in VO_2 films based on the analysis of the perimeter of fractal figures P as a function of their area A. This approach is described in most monographs on fractals, in particular in [3, 4]. It was originally used for the analysis of the fractal dimensions of clouds. It was also applied in [1] to analyze the shape of metallic and dielectric inclusions during MIT in VO_2. In this approach, the dimension of a fractal object boundary D is determined from the slope (magnitude of the derivative) of the dependence $P(A)$ in double logarithmic coordinates. This dependence has the following form:

$$P(A) = \beta A^{D/2} \text{ or } \log P = \log\beta + \frac{D}{2}\log A \,. \tag{1}$$

Hence, for the fractal dimension of a contour we have

$$\frac{D}{2} = \frac{d\log P}{d\log A}. \tag{2}$$

Here, d corresponds to differentiation.

For Euclidean figures $D/2 = 0.5$. Exceeding this threshold indicates the fractality of objects. Even if the figures (including the Euclidean ones) are not quite similar to each other (the shape coefficient β varies in a certain range), this leads only to an increase in the scatter of the experimental points, while maintaining the overall value of the slope. If the slope changes upon increasing (decreasing) the object size, we can say about multifractality of the investigated family. Most often, the available image resolution does not allow us to reliably detect fractality (ruggedness) of the contour of small-size areas, even if it is actually present.

3. Brief description of the created software

The analyzed image is converted to the black and white one. Then using filters, the boundaries of the objects with different thresholds are identified. Depending on the image, three types of filters were used, namely: Sobel, Prewitt and combined one [12], combining both approaches.

As a result, each pixel of the image is assigned to the figure boundaries, figure inner region or the outer region of the background outside all the enclosed regions. Then a special algorithm detects each such region (as well as its protruding fragments) and finds the rectangle encompassing it. Then the perimeter P_i and the area A_i are determined just by pixel counting inside the enclosing rectangle. The pixels belonging to the boundary of the i-th shape give the perimeter, and the pixels of the inner region give its area. The pair of the values $\{A_i, P_i\}$ thus corresponds to one experimental point of the dependence $P = f(A)$. After removing duplicates, a regression curve of the form (1) is constructed by the least square method in double logarithmic scale. The angular coefficient of this log-log plot is a half of the fractal dimension D for the contour of the figures.

The results of testing our program on Euclidean figures and a number of classical fractals showed excellent agreement with the predicted values of fractal dimension. Processing of the image from [1] resulted in $D = 1.48116$, which is very close to the authors' result (1.488), while Gwyddion (using the cube counting method) outputs 1.41 for this case and about 1.3 for a set of Euclidean figures.

4. Experimental

VO_2 films were grown on (111) Si substrates by magnetron sputtering of VO_2 [13]. Prior to the film deposition, the chamber was pumped out to the pressure of $(1...2)\cdot10^{-5}$ Torr. During the deposition process, the Ar pressure (99.999% purity) was maintained at $(2...4)\cdot10^{-3}$ Torr. The magnetron power was 50...70 W, and the substrate temperature was 235 ± 15 °C. After deposition, the samples were annealed at 350 °C for 30 h in Ar environment. After annealing, the next layer of VO_x was deposited on the surface, and the samples were annealed again. This allowed one to deposit thicker films with good adhesive properties as well as to use already deposited crystalline films as recrystallization centers. The first deposited layer mainly contained the V_4O_9 phase and did not undergo MIT. In the present work, we considered the films containing three (Fig. 1) and two layers (Fig. 2). Scanning electron microscopy images were acquired using a MIRA 3 TESCAN equipment. The surface nanorelief of the annealed vanadium dioxide films was studied using atomic force microscopy (AFM) on a scanning probe microscope NanoScope IIIa Dimension 3000TM. The measurements were performed in the tapping mode by using ultrasharp silicon probes with the nominal tip radius of 8 nm.

It can be seen that the film morphologies and their resistance-temperature dependences $R(T)$ are substantially different. In particular, the film with lens-like inclusions (three-layer) has zero temperature hysteresis of resistance (Fig. 1a). In contrast, the films with stellar and lamellar inclusions (two-layer) show a pronounced hysteresis (Fig. 2a). We note that lens-like inclusions quite often form fractal structures during martensitic phase transition in metals [14].

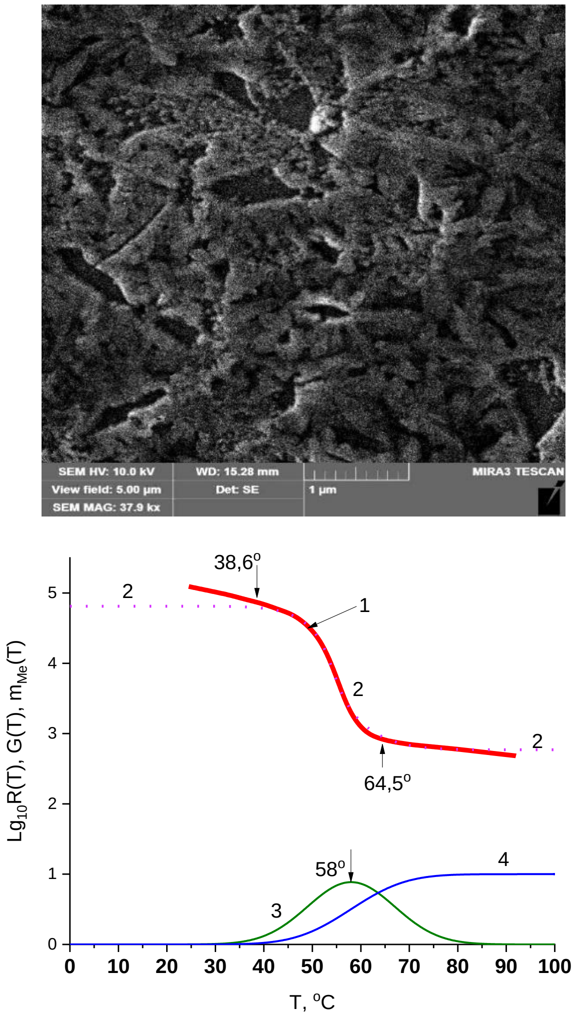

Fig. 1. Scanning electron microscopy image of the surface of the film containing lens-like inclusions (a) and the temperature dependence of resistance $R(T)$ without hysteresis observed for this film (b). Here, *1* – experimental dependence, *2* – dependence of the resistance calculated by the random medium model, *3* – calculated temperature distribution of MIT in the film $G(T)$, and *4* – calculated temperature dependence of the fraction of metallic phase m_{Me} (T).

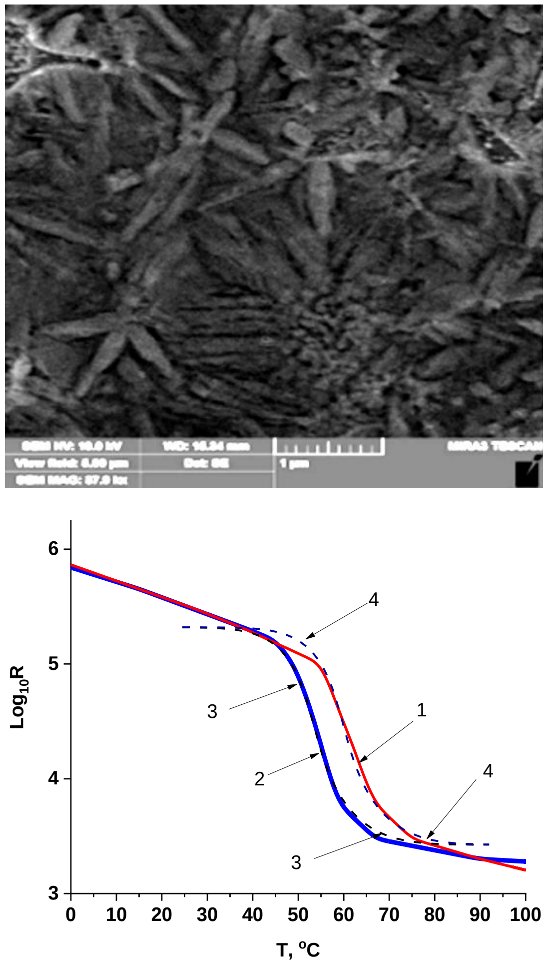

Fig. 2. Scanning electron microscopy image of the surface of the film containing both stellar and lamellar inclusions (a) and the temperature dependence of resistance $R(T)$ with hysteresis in the vicinity of MIT (b) observed for this film. Here, *1* and *2* are the experimental dependences during heating and cooling, *3* and *4* are the corresponding resistivity dependences calculated by the random medium model.

5. Fractal analysis of images of the studied samples

Figs 3 and 4 show the results of processing two images of the VO_2 films with significantly different topologies (“lenses” and “stars”) and different resistivity hysteresis using the Gwyddion software. Despite the significant differences in the surface morphology of these films, the results of determining the fractal dimension provided by this software were almost identical. This applies not only to the cube counting method, but also to all the methods implemented in it [6], except for the power spectrum method.

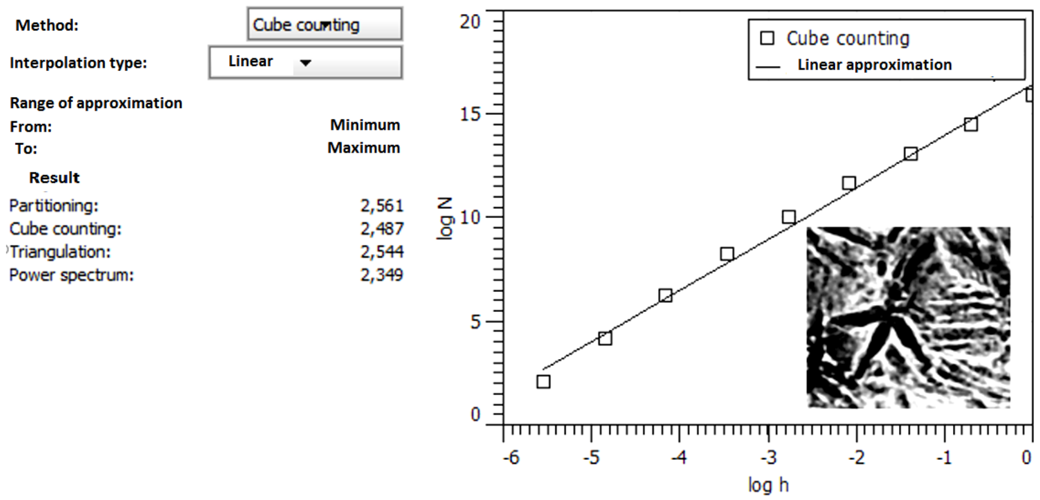

Fig. 3. Results of image processing of VO_2 film (Fig. 2a) obtained by Gwyddion 2.50 program. Fractal dimension of the contour of stellar inclusions D = 1.487.

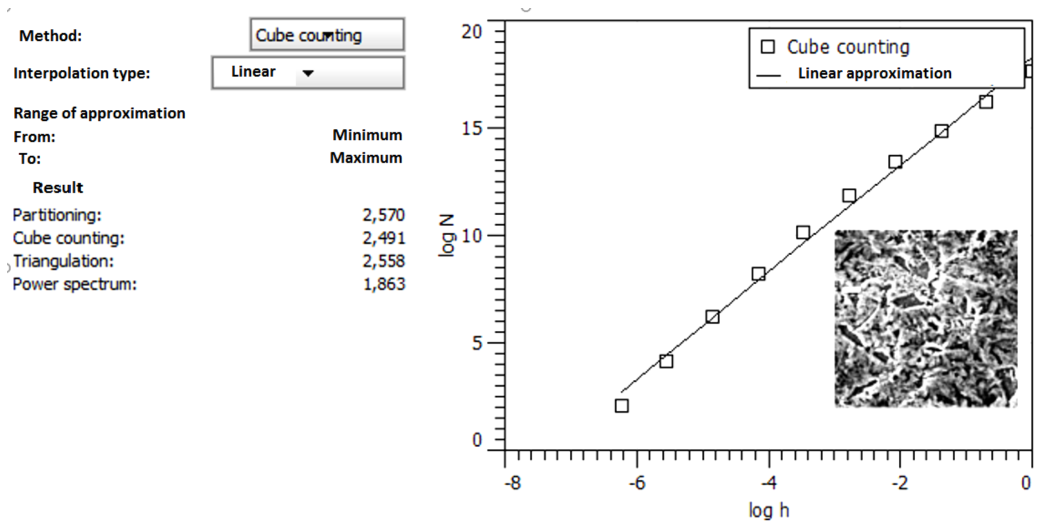

Fig. 4. Results of image processing of VO_2 film (Fig. 1a) obtained by Gwyddion 2.50 program. Fractal dimension of the contour of lens-like inclusions D = 1.491.

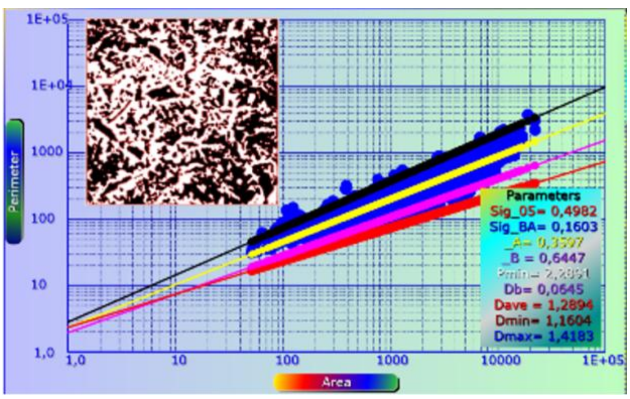

Fig. 5. Results of processing the VO_2 film image (Fig. 1a) by our software. The fractal dimension of the contour of lens-like inclusions D = 1.2894. (Color online)

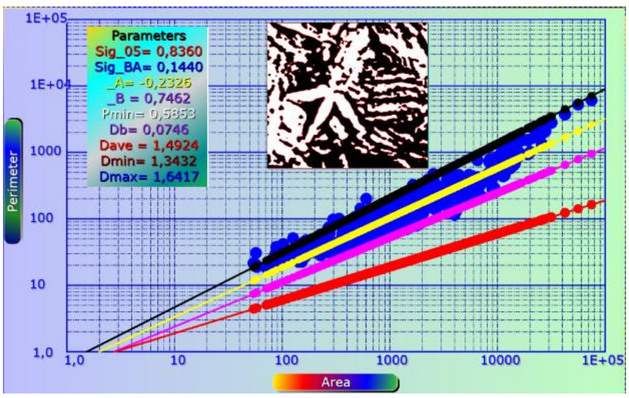

Fig. 6. Results of processing the VO_2 film image (Fig. 2a) by our program. The fractal dimension of the contour of stellar-like inclusions D = 1.4924. (Color online)

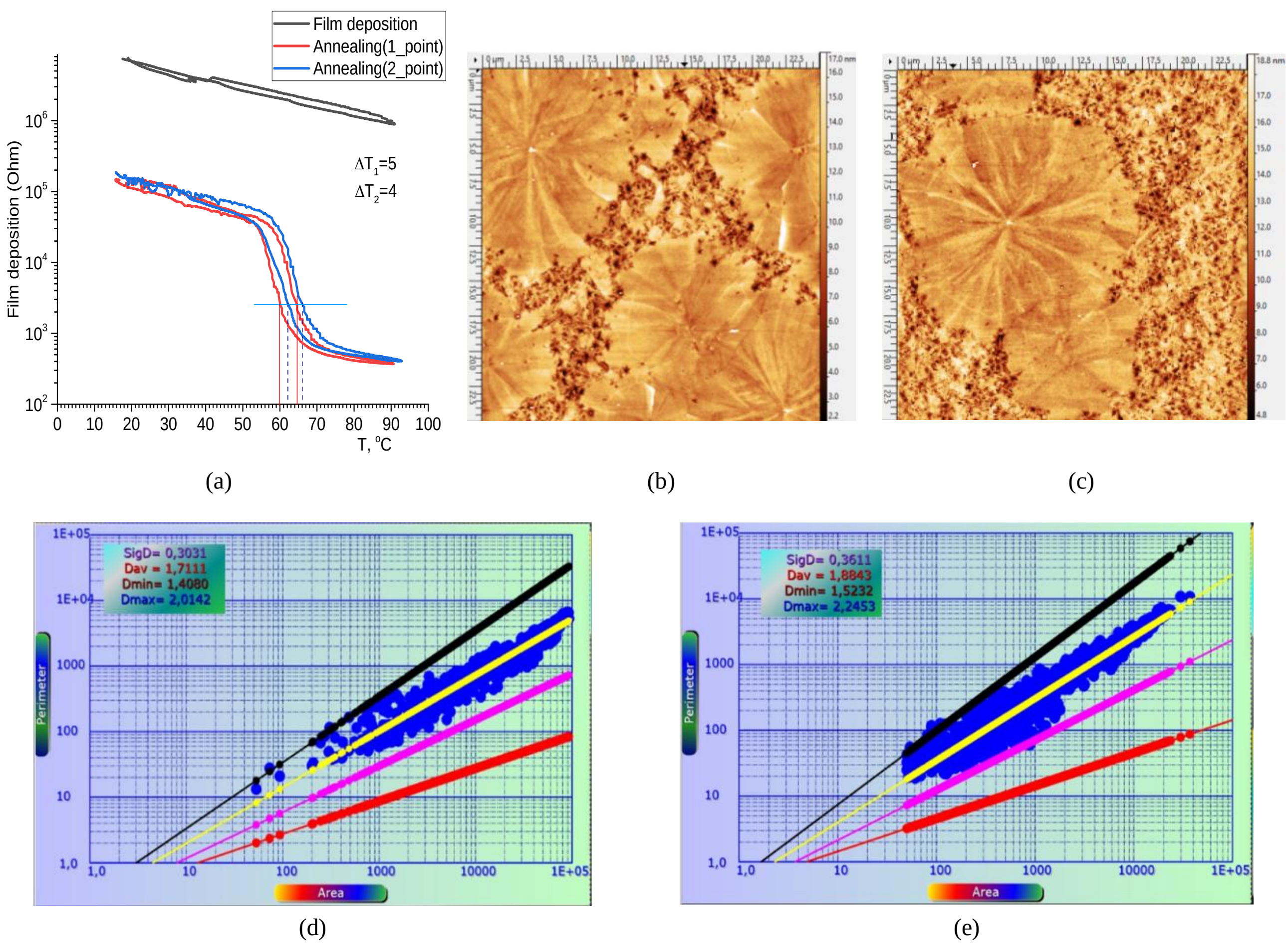

Fig. 7. Evolution of the shape of the $R(T)$ curve during annealing of VO_2 film in comparison with the change of the fractal dimension of surface morphology. Here, (a) are the $R(T)$ dependences for the nonannealed film (black curve) and after annealing (red and blue ones); (b) and (c) – scanning probe microscopy images of two different spots of the film surface after annealing. Determination of the fractal dimension (d) and (e) from the images (b) and (c). (Color online)

Figs. 5 and 6 show the same images processed by our software. The yellow color shows the most probable approximation of the experimental points obtained by the least square method. The purple and black lines correspond to restricting the point family from above and below within the spread ±σ. The red line corresponds to the hypothetical case when all the analyzed figures are purely Euclidean.

For each of these two cases, markedly different fractal dimension values were obtained, which is consistent with the apparent differences in the film morphology and conductivity. Comparing two softwares used, we can conclude that for the considered problem, comparison of the area and perimeter of inclusions seems to be the best method for determining the fractal dimension. Such method unmistakably recognizes the figures with Euclidean contour and at the same time easily handles classical fractals like coastlines. For significantly different film morphologies, it also results in different fractal dimensionalities, while other methods of fractal analysis only partially succeed. Fig. 7 shows the results of the comparison of the hysteresis curves $R(T)$ at the fractal dimensions determined from the surface images of another group of samples before and after annealing.

The freshly prepared film shows an exponential dependence of the resistance drop with increasing temperature. Over the entire temperature range (both heating and cooling), this film remains dielectric and does not demonstrate any MIT (Fig. 7a). Annealing modifies the film, creating a heterogeneous morphology in it (Figs 7b and 7c) with a rather high fractal dimension, the value of which is different in different surface areas. At some sites $D = 1.711$ (Fig. 7d) and at other ones $D = 1.884$ (Fig. 7e). In this case, a pronounced MIT with noticeable hysteresis is observed (Fig. 7a). We can also see here that a larger hysteresis of $R(T)$ corresponds to a larger value of D.

The results obtained by mathematical processing of surface images showed that crystallites in the films are pronounced fractal objects, the fractal dimensions D of which approach 1.5 and in some cases exceed this value. A correlation between the fractal dimension, film morphology, and behavior of the temperature dependence of resistivity during MIT was found. Higher fractal dimension of the surface morphology elements corresponds to a wider hysteresis of the $R(T)$ dependence.

6. Calculation of elastic stress in the film structures at different crystallite shapes

As noted by many authors, MIT in VO_2 is much similar to martensitic transformations [15, 16]. In accordance with the general ideas about martensitic transformations [17], in some cases increase of the elastic energy caused by appearance of a new phase can compensate the thermodynamic gain associated with the phase transition itself. As a result, growth of a new phase stops.

The tendency of elastic energy minimization during martensitic transformations makes the inclusions of a new phase have the shape of plates oriented in a special way relative to the crystallographic axes of the initial lattice. The tendency to reduce the intrinsic elastic energy leads to partitioning of the new phase into the domains shifted or rotated relative to each other. If the strain tensor contains a shear component, the domain shape corresponding to the strain energy minimum is a plate with a small ratio of thickness to other dimensions. In reality, such domains often have the shape of a thin lens oriented in a certain way in the crystal [14].

Reduction of the elastic energy of the system also occurs by partition of lamellar (lens-like) crystals into even thinner plane-parallel domains (twins) that mutually compensate each other's elastic fields. It may be assumed that fractal objects are also capable of effectively relaxing elastic stress in a solid body. This section presents the results of numerical modeling of elastic fields in a VO_2 film containing inclusions of a quasi-fractal shape that have either a developed boundary of the stellar type or represent an ensemble of oriented in a certain way lens-like inclusions. Such structures were observed experimentally and analyzed above with respect to the fractal dimension of the boundaries. The calculations were performed using the COMSOL® Multiphysics® software. Without limiting generality, it was assumed that the film was subjected to external tensile load due to the presence of the substrate. We analyzed how effectively the elements of the fractal geometry, such as "fringing" and/or roughness of the inclusion boundary, can contribute to relaxation of the tensile stress in a certain region of the film and, thus, affect the phase transition conditions in this region.

When calculating the stress field created in the matrix (VO_2 in monoclinic structure) by inclusions of the second phase (VO_2 in tetragonal structure), the limiting option was chosen that these inclusions affect the matrix as strongly as possible. For this purpose, cavities similar in shape to the inclusions observed experimentally were placed into the stretched film.

Figs 8 and 9 show maps of the distribution of elastic compression and tension stress fields in the vicinity of quasi-fractal objects with different boundary topologies. These maps show not only the regions of complete stress relaxation (dark orange, the stress is equal to zero) but also the regions of compression (red) and stretching (blue). Figs 8 and 9 show that the stellar-like structures create within themselves (between their rays or boundary relief protrusions) the regions with zero elastic energy, where the external elastic stress is completely relaxed. At the same time, the ray tips serve as concentrators of stress of different signs, which can change the local temperature of MIT in either direction from the equilibrium value for an unstressed sample.

Figs 10 and 11 show that effective stress compensation in the vicinity of quasi-fractals with a "fringed" and rough boundary is achieved only if the period of the protrusions is sufficiently small. Otherwise, the unstressed regions (orange) contain nonrelaxed areas in the centers between the relief protrusions. In these areas, the stress relaxes only partially. The fact that the degree of stress field relaxation depends on the boundary relief period will be used below in the analytical model. However, as shown in Fig. 11, even the initial stages of the formation of an additional tree-type fractal structure on the boundary relief protrusions lead to almost total compensation of this small residual stress.

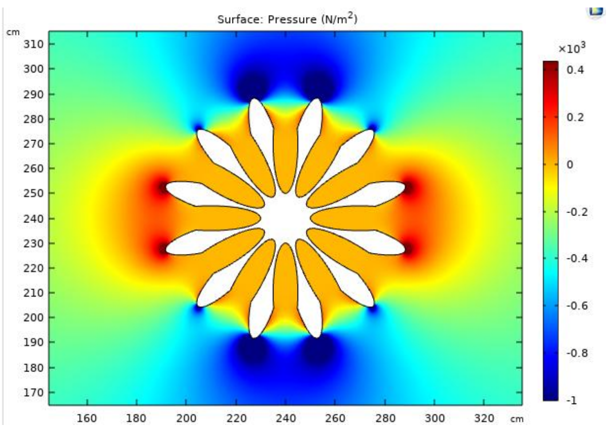

Fig. 8. Compression and tension distribution in the vicinity of a stellar-like inclusion with a smooth boundary of variable curvature. (Color online)

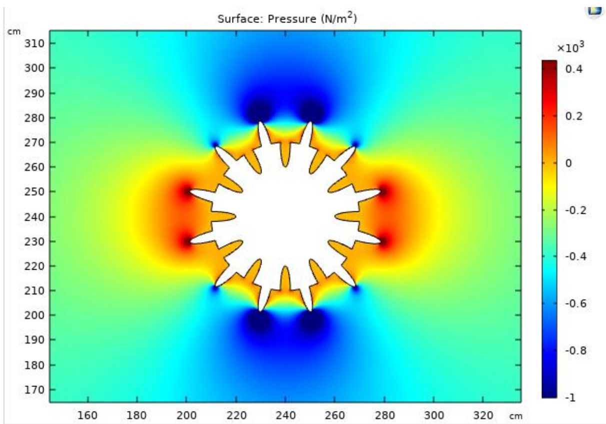

Fig. 9. Compression and tension distribution in the vicinity of an inclusion with "fringed" rugged boundary. (Color online)

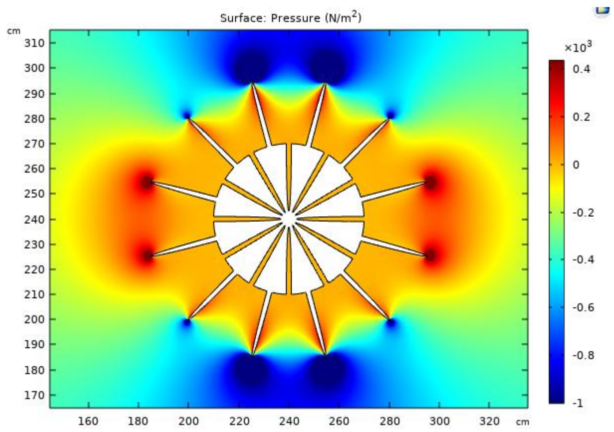

Fig. 10. Compression and tension distribution in the vicinity of a stellar-like inclusion with indented boundary and sharp protrusions (stress concentrators of both signs). (Color online)

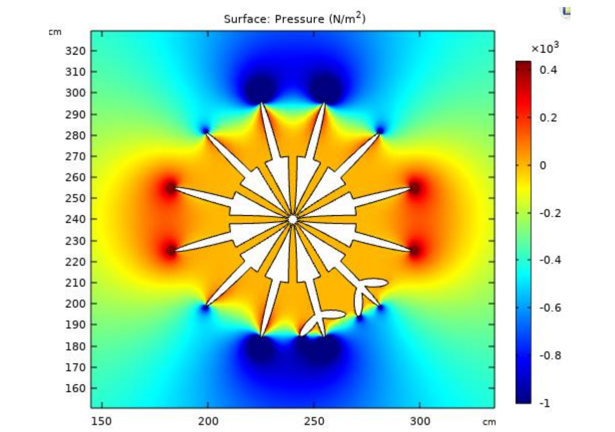

Fig. 11. Correction of the elastic field in the vicinity of a stellar-like inclusion with a rugged boundary at appearance of additional branches on the protrusions of the boundary relief. (Color online)

Similar calculations of elastic stress relaxation inside the fractal ensemble of lens-like inclusions ([14], Fig. 21a) showed that already at the first stage of fractal formation, a significant part of the surface inside the triangular region bounded by three lenses relaxes significantly. As the fractal grows (by repetitively adding smaller lenses into the gaps between the larger lenses), the effect becomes even stronger and the region with zero elastic energy uniformly fills the entire inner space of the ensemble. This result is similar to the effect observed in Fig. 11. Namely, appearance of small structural elements in the vicinity of larger ones leads to a more complete and uniform stress relaxation over the volume.

7. Analytical model for calculating the system free energy as a function of the fractal dimension of new phase inclusions

In this section, we consider the following questions: Why do the inclusions of a new phase and the crystallites themselves in VO_2 films have fractal shapes with certain quantitative characteristics in our case of MIT, and what is the mechanism of the appearance of fractal objects, in particular for metal-dielectric phase transitions? It seems that the Euclidean shape with a smooth boundary of the minimum perimeter should provide the optimal shape of inclusions of a new phase.

The question of “zigzag” interphase boundaries in solids was first considered by Roytburd in the framework of a simple model [18]. It was shown that appearance of boundaries is a consequence of the instability of a single-phase state under the action of a long-range (in particular, elastic) field generated by this serrated interphase boundary. The ratio of the period of teeth h to the zigzag boundary thickness l (*i.e.* the relief span) is determined by competition of two factors, namely the elastic energy of stress created by the sides of the teeth and the surface energy. For thin teeth ($h/l \ll 1$), the elastic stress is proportional to the deflection of the tooth sides from the plane, where the mutual phase distortion is minimized.

Therefore, the elastic stress is proportional to h/l, and the elastic energy is the smaller, the smaller is h. This conclusion is also confirmed by our numerical calculations described in the previous section. As the period of the boundary roughness decreases, the fraction of the film volume where the stress is absent or small increases. On the contrary, the surface (interface) energy grows with decreasing the tooth thickness h, *i.e.*, with increasing the number of relief protrusions per unit length of the smoothed boundary. The author gives the following approximate expression for the free energy per unit length of a zigzag boundary:

$$F = e(h/l)^2 l + 2\gamma(l/h)\,. \qquad (3)$$

Here, e and γ are the specific elastic (per unit area) and surface (per unit perimeter length) energies.

Minimizing this expression by h, we obtain the equilibrium ratio $h/l = (\gamma/el)^{1/3}$, from which the local free energy minimum $F = F(h/l)$ is found. Hence, an inclusion with a rough boundary may be in principle stable. This simplified approach gives us the main idea: the elastic energy decreases with decreasing the roughness period of the boundary h, while the total perimeter of a new phase inclusion (and the interphase energy) grows. Let us apply this approach to a fractal inclusion of a new phase. For such an object, both the boundary roughness and its length (inclusion perimeter) P grow upon increasing the fractal dimension. In particular, $P = \alpha R^D$, where R is the characteristic transverse dimension of the inclusion. Note that the appearance of the fraction dimension D does not affect the physical dimension of the perimeter value (it remains the length), but concerns only its numerical value.

If we approximate a fractal object by an equal-sized Euclidean figure with a smooth boundary and perimeter $P_E = \alpha_E R$, the inverse of the roughness period (frequency of relief protrusions) will be equal to

$$h^{-1} \approx \frac{1}{2l}\frac{P}{P_E} = b\frac{R^{D-1}}{2l}\,. \qquad (4)$$

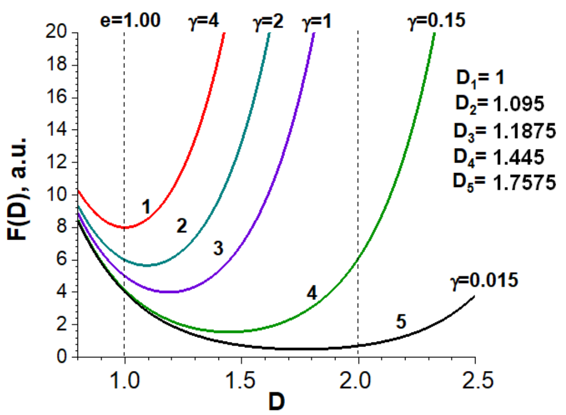

Fig. 12. Dependence of the fractal inclusion free energy *F* and its components on the fractal dimension *D* at different values of the interface energy γ. *1–5* – total free energy *F*(*D*) at different γ. Curve *1* corresponds to a stable inclusion of the Euclidean shape. The minimum positions of *F*(*D*) for each curve are indicated.

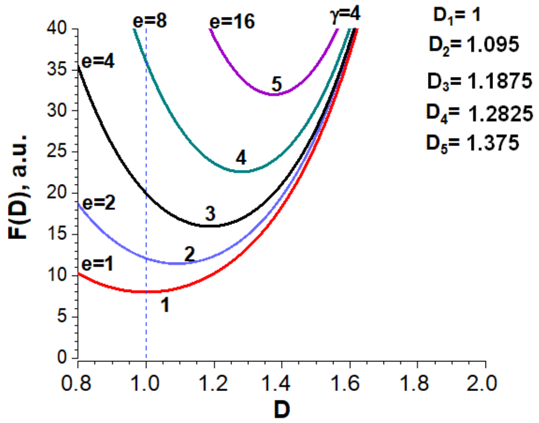

Fig. 13. Dependence of the fractal inclusion free energy *F* and its components on the fractal dimension *D* at different values of elastic energy *e*. *1–5* – total free energy *F*(*D*) at different *e*. Curve *1* corresponds to a stable inclusion of the Euclidean shape. The minimum positions of *F*(*D*) for each curve are indicated.

Here, *l* is again the average roughness spread or the thickness of the notched interface boundary. It can be seen that the roughness frequency also increases upon increasing the fractal dimension *D*. We note that since the considered figures are equal-sized, the coefficient $b = \alpha/\alpha_E \approx 1$.

Using the Roytburd formula (3), the free energy of a fractal object in a solid-state matrix can be approximated as follows:

$$F = e\left(\frac{2}{bR^{D-1}}\right)^2 l + \gamma b R^{D-1}. \tag{5}$$

We see that the elastic component of the free energy decreases rapidly with increasing the fractal dimension, but the interface component increases. The result also depends on the size of the inclusion *R* as well as on the boundary roughness *l*, which in turn implicitly depends on the fractal dimension. Taking into account that in this case the contour tortuosity is also a consequence of fractality (deviation of the figure from the Euclidean shape), as a first approximation $l \sim \kappa R^{D-1}$ may be accepted, where κ is another shape coefficient. Finally, we obtain that the elastic summand in the free energy decreases as $1/R^{D-1}$ and the interface summand increases as R^{D-1}. Taking into account that *b* is close to unity, we finally have

$$F = e\left(\frac{4\kappa}{R^{D-1}}\right) + \gamma R^{D-1}. \tag{5a}$$

In this simple model, the fractal dimension acts as the only control parameter that sets equilibrium inclusion shape. Qualitative dependence of the free energy *F* on the fractal dimension *D* is presented in Figs 12 and 13. It follows from these graphs that:

1) At a certain ratio between the specific energies, the minimum of the system free energy corresponds exactly to $D = 1$. In such a system, no stable fractal inclusions of a new phase can form. (Fig. 12, curve *1*, Fig. 13, curve *1*.)

2) If we fix the specific elastic energy *e* and decrease the interface energy γ, the minimum of the *F*(*D*) curve shifts to larger values of the dimension *D*, and the minimum itself becomes deeper and wider (Fig. 12). At small γ, the system consisting of high-dimensional fractal inclusions ($D \sim 1.4\ldots1.75$) becomes anomalously stable. However, the broad minimum of *F*(*D*) means that a larger spread of fractal dimension should be expected, since the clusters with *D* in the range of 1.5 to 1.9 have close free energies (Fig. 12, curve *5*).

3) If, on the contrary, the specific interface energy is sufficiently large, growth of the inclusion perimeter due to the growth of *D* will quickly cancel out the achieved elastic energy gain. In this case, the minimum of *F*(*D*) will shift toward more and more Euclidean shapes. At a certain ratio ($\gamma/e = 4$ in our case), formation of fractals becomes energetically unfavorable ($D = 1$).

4) If we fix γ and increase the specific elastic energy *e* (Fig. 13), *e.g.* by introducing impurities of a large radius or by adding external elastic stress sources, *D* will increase weakly from unity to about 1.4, the free energy minimum will narrow, and the energy at the minimum will grow because of the pumping the elastic energy into the system. At the same time, *D* will have a small variation. Hence, a weak fractality can be induced in the system by increasing the role and influence of elastic fields.

5) According to the formula (5a), size dependence of *F* is expressed as R^{D-1}. Therefore, for shapes close to the Euclidean one, the minimum position of *F*(*D*) weakly depends on the characteristic dimension. On the contrary, when the fractal dimension of equilibrium inclusions

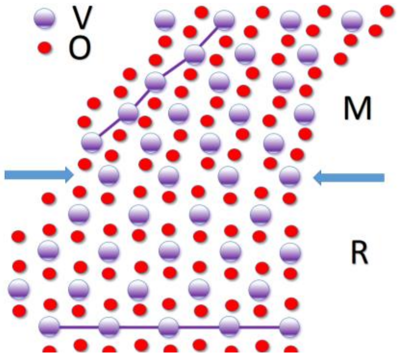

Fig. 14. Principal possibility of coexistence of inclusions of two phases, M and R, in the presence of a coherent boundary between them. (Shown by arrows)

approaches one and a half and higher, stable inclusions of different sizes will also have slightly different boundary indentation degrees, the greater, the smaller are the sizes. This can be clearly seen from the experimental "area *versus* perimeter" relationships in Figs 5–7. In the small size region, the $\log P(\log A)$ points lie predominantly above the regression curve. This trend is particularly noticeable in Fig. 7e, where the average value of $D > 1.8$.

It follows from the above that MIT has indeed all prerequisites for formation of fractal objects, since the boundaries between the inclusions of metallic and dielectric phases are often coherent (Fig. 14), *i.e.*, the interphase energy is small. Comparing the crystal lattices of the monoclinic (M) and rutile-like (R) metallic phases, it can be seen that the transition R↔M occurs with minimal changes in the interatomic distances. In the rutile (tetragonal) phase, vanadium atoms form rectilinear rows with $d_{V\text{-}V} = 2.88$ Å. In the monoclinic phase, vanadium atoms form zigzag chains with $d_{V\text{-}V} = 3.16$ Å. The pairwise spacing in the M phase is $d_{P\text{-}P} = 2.62$ Å. [19]. At the same time, both phases can be docked with each other almost without boundary distortion by a suitable mutual orientation of the inclusions as can be seen in Fig. 14.

As can be seen from Fig. 12, the initial phase is more stable at higher fractal dimensions, and the transition metal ↔ dielectric will require stronger overheating and overcooling. Consequently, one may expect a wider hysteresis on the $R(T)$ dependence.

8. Discussion of physical results

Thus, the reason for the appearance of stable fractal structures during MIT is the unique ratio between the elastic and interface specific energies in VO_2 at the boundary between two coexisting phases. The elastic interaction decreases when the inclusion boundaries become tortuous (fringe-shaped) and, in the limiting case, additionally roughened. On the other hand, the interface energy is proportional to the perimeter. Therefore, it can be minimal only when the inclusion has a smooth rounded shape and increases rapidly with the increase of the boundary ruggedness, *i.e.* its fractal dimension. In the simplest case we have two concurrent contributions to the free energy, namely from the long-range elastic forces and local interface interaction. The free energy minimum is achieved at some optimal value of D, when both effects are balanced.

However, as shown by the modeling results, an object does not have to be an ideal self-similar fractal at all observable scales. Simple star-like shapes, specifically arranged lenses and other similar elements with hierarchically decreasing dimensions also effectively reduce the elastic energy of the system. This is due to the well-known effect of "stress relief". The stress generated by large inclusions can be compensated (or the solid may be unloaded) by adding suitable smaller inclusions to their vicinity. In its turn, the uncompensated residual stress generated by these small inclusions can be compensated by even smaller suitably located inclusions.

A fractal has the advantage that it initially comprises all the structural elements of all sizes from the largest to the smallest ones. Moreover, these elements are hierarchically located in the most suitable places relative to each other. This allows stress relief to be distributed over larger areas, while simultaneously making the stress relaxation more uniform in space (Fig. 11). At each generation of the fractal growth, more and more small elements are formed, each of which relaxes the stress generated by the fractal fragments of the previous generation. Finally, the smallest fragments of the boundary become the stress concentrators. The stress becomes localized in small regions of the solid (Figs 8–11) without significantly affecting nucleation in the rest of the matrix. As a result, the deepest possible effect of elastic stress relaxation in the system as a whole is achieved.

Although in the simple model proposed here the fractal dimension is the only controlling parameter, in the general case the situation may be more complicated. Since everything depends on the mutual arrangement of individual elements and a certain hierarchical ratio of their sizes, we can assume that the fractal dimension is not the only geometrical parameter determining the minimum free energy of the system. One can expect a certain influence of other topological parameters, including fractal dimensions of higher orders, mutual arrangement of fractal regions, *etc*.

9. Conclusions

The main mechanism leading to the fractal shape of new phase inclusions during the metal-insulator transition in VO_2 films has been revealed. It consists in the fact that the inclusions of a new phase with a fractal shape of the boundary significantly reduce (down to zero) the elastic stress in their vicinity, thereby reducing the elastic energy of the system. Although topologically complex interphase boundaries are formed at this, their contribution to the total free energy of the system is small due to their small specific interphase energy. This is a characteristic feature of coherent boundaries between the monoclinic and rutile phases. We have presented the data on the topology of the VO_2 films, which are compared with the temperature dependences of the resistivity of these films $R(T)$ in the vicinity of MIT. It is shown that in our case the topology, morphology and texture of the film noticeably affect the value of the hysteresis $R(T)$. Based on the literature data, we have attempted to relate the structural parameters of the films to their electrical characteristics based on the fractal dimension of the film structural elements. To determine the fractal dimension from images, we used both the well-known Gwyddion software as well as the author's own development, which showed the best results on the test images. It turned out that the investigated VO_2 films demonstrated fractal dimensions of the boundaries of their constituent structural elements in the range of 1.4 to 1.5 and higher.

This kind of a "non-Euclidean" shape of both nuclei of the new phase and film grains testifies the dominant role of elastic stress during MIT. This fact was verified by numerical modeling of elastic fields in the vicinity of inclusions with quasi-fractal boundaries. The modeling was carried out using the COMSOL® Multiphysics® software. It was shown that the elements with fractal boundaries as well as the fractals consisting of suitably arranged Euclidean figures (*e.g.*, lenses) with hierarchically decreasing dimensions fully or partially relax elastic stress in the vicinity of the inclusion, facilitating phase transition. Based on these results, we have proposed an analytical model that allowed us to relate the free energy of the film F to the fractal dimension D of the structural elements of its components. It is shown that depending on the ratio between the elastic and interface specific energies, the position of the free energy minimum $F(D)$ is defined by a certain optimal fractal dimension. The depth of the energy minimum also varies making the phase more stable at higher fractal dimensions. It follows from the model, in particular, that at a certain threshold ratio between the specific elastic and interphase energies, formation of stable fractal nuclei with the dimension of the boundary $D > 1$ is fundamentally impossible. Therefore, such nucleation in VO_2 during MIT is a unique feature of this material, which is caused by the small value of the interface energy and the presence of coherent boundaries between the metallic and dielectric phases (Figs 12–14). This conclusion explains well the experimentally observed relationship between the morphology of vanadium dioxide films and the features of the hysteresis loop on the $R(T)$ dependence. It significantly extends the concept of the nature and mechanism of the influence of the structure and morphology of VO_2 films on the MIT parameters proposed earlier in [19–22].

References

1. Sohn A., Kanki T., Sakai K. *et al.* Fractal nature of metallic and insulating domain configurations in a VO_2 thin film revealed by Kelvin probe force microscopy. *Sci. Rep.* 2015. **5**. P. 10417. https://doi.org/10.1038/srep10417.
2. Qazilbash M.M., Brehm M., Chae B.G. *et al.* Mott transition in VO_2 revealed by infrared spectroscopy and nano-imaging. *Science*. 2007. **318**, No 5857. P. 1750–1753. https://doi.org/10.1126/science.1150124.
3. Feder J. *Fractals*. New York, Springer, 1989.
4. Mandelbrot B.B. *Fractal Geometry of Nature*. New York, Henry Holt and Company, 1983.
5. Krasikova I.E., Krasikov I.V., Kartuzov V.V. Correlation of values of fractal characteristics of the material's structure based on the electron-microscopic images of the sample surface with the values of their physical and mechanical properties. *Electron Microscopy and Strength of Materials*. 2016. **22**. P. 3–10. http://dspace.nbuv.gov.ua/handle/123456789/125899.
6. Klapetek P., Nečas D., Anderson C. *Gwyddion user guide*. 2004-2007, 2009-2023.
7. Douketis C., Wang Z., Haslett T.L., Moskovits M. Fractal character of cold-deposited silver films determined by low-temperature scanning tunneling microscopy. *Phys. Rev. B*. 1995. **51**, No 16. P. 11022–11031. https://doi.org/10.1103/PhysRevB.51.11022.
8. Zahn W., Zösch A. The dependence of fractal dimension on measuring conditions of scanning probe microscopy. *Fresenius J. Analen. Chem*. 1999. **365**. P. 168–172. https://doi.org/10.1007/s002160051466.
9. Van Put A., Vertes A., Wegrzynek D. *et al*. Quantitative characterization of individual particle surfaces by fractal analysis of scanning electron microscope images. *Fresenius J. Analen. Chem*. 1994. **350**. P. 440–447. https://doi.org/10.1007/BF00321787.
10. Mannelquist A., Almquist N., Fredriksson S. Influence of tip geometry on fractal analysis of atomic force microscopy images. *Appl. Phys. A*. 1998. **66**. P. 891–895. https://doi.org/10.1007/s003390051262.
11. Zahn W., Zoesch A. Characterization of thin film surfaces by fractal geometry. *Fresenius J. Anal. Chem*. 1997. **358**. P. 119–121. https://doi.org/10.1007/s002160050360.
12. Gonzalez R.C., Woods R.E. *Digital Image Processing* (4th ed.). Pearson Education Limited, 2018.
13. Kladko V.P., Melnik V.P., Liubchenko O.I. *et al*. Phase transition in vanadium oxide films formed by multistep deposition. *SPQEO*. 2021. **24**, No 4. P. 362–371. https://doi.org/10.15407/spqeo24.04.362.
14. Hornbogen E. Fractals in microstructure of metals. *Int. Mater. Rev*. 1989. **34**, No 6. P. 277–296. https://doi.org/10.1179/imr.1989.34.1.277.
15. Huang F., Gong M., Tian S. *et al.* Controlling the crystalline orientation and textual morphologies of the VO_2 film and the effect on insulator-metal transition properties. *Jpn. J. Appl. Phys*. 2022. **61**. P. 085504. https://doi.org/10.35848/1347-4065/ac7c4c.

16. Khakhaev I.A., Chudnovsky F.A., Shadrin E.B. Martensite effects for metal-dielectric phase transition in vanadium dioxide films. *Solid State Physics*. 1994. **6**. P. 1643–1649.
17. Ainabayev A., Mullarkey D., Walls B. *et al*. Epitaxial grown VO_2 with suppressed hysteresis and low room temperature resistivity for high-performance thermal sensor applications. *ACS Appl. Nano Mater*. 2023. **6**. P. 2917–2927. https://doi.org/10.1021/acsanm.2c05297.
18. Roytburd A.L. Instability of border regions and formation of zigzag interdomain an interphase boundaries. *Lett. ZhETF*. 1988. **47**, No 3. P. 141–143.
19. Narayan J., Bhosle V.M. Phase transition and critical issues in structure-property correlations of vanadium oxide. *J. Appl. Phys.* 2006. **100**. P.103524. https://doi.org/10.1063/1.2384798.
20. Atkin J.M., Berweger S., Chavez E.K. *et al*. Strain and temperature dependence of the insulating phases of VO_2 near the metal-insulator transition. *Phys. Rev. B.* 2012. **85**. P. 020101(R). https://doi.org/10.1103/PhysRevB.85.020101.
21. Liubchenko O., Kladko V., Melnik V. *et al*. Ar-implanted vanadium dioxide thin film with the reduced phase transition temperature. *Mater. Lett*. 2022. **314**. P. 31895. https://doi.org/10.1016/j.matlet.2022.131895.
22. Lytvyn P.M., Dzhagan V.M., Valakh M.Ya. *et al.* Nanomechanical properties of polycrystalline vanadium oxide thin films of different phase composition. *SPQEO*. 2023. **26**, No 4. P. 388–397. https://doi.org/10.15407/spqeo26.04.388.

Authors and CV

Alex A. Efremov, PhD in Physics and Mathematics (1990), Senior Researcher at the V. Lashkaryov Institute of Semiconductor Physics. His scientific interests include computer simulations and modeling in nanophysics and technology of semiconductors and related materials. He authored over 80 scientific papers.
https://orcid.org/0000-0001-9608-6571

Boris Romanyuk defended his Dr.Sci. thesis in 1980 (Physics and Mathematics) at the V. Lashkaryov Institute of Semiconductor Physics. He is the Head of the Department of Ion-Beam Engineering and Structural Analysis at the same institute. Author of more than 270 scientific publications. His research interests include physics of semiconductors and dielectrics, ion-beam engineering and wide-range studies of semiconductor structures.
E-mail: romb@isp.kiev.ua,
https://orcid.org/0000-0002-1688-7588

Viktor Melnik, Professor, acting director of the V. Lashkaryov Institute of Semiconductor Physics. He defended his Dr.Sci. thesis in 2012 (Physics and Mathematics) at the V. Lashkaryov Institute of Semiconductor Physics. Author of more than 250 scientific publications. His main research activity is in the fields of ion-beam engineering and diagnostics. E-mail: vp_mel@ukr.net,
https://orcid.org/0000-0002-8670-7415

Oleksandr A. Stadnik, PhD in Physics and Mathematics, Deputy Head of the Department of Ion-Beam Engineering and Structural Analysis of the V. Lashkaryov Institute of Semiconductor Physics. His research interests include molecular-beam epitaxy, analysis of the surface structure of semiconductor crystals, hetero- and nanosystems.
E-mail: stadnyk.o@gmail.com

Tomash Sabov, PhD in Physics and Mathematics (2019) at the Department of Ion-Beam Engineering at the V. Lashkaryov Institute of Semiconductor Physics. He is the author of more than 20 publications. His main research activity is physics of thin films, chromogenic materials and SIMS analysis.
E-mail: tsabov92@gmail.com
https://orcid.org/0000-0003-2636-2379

Oleksandr A. Kulbachynskyi, PhD student at the Department of Ion-Beam Engineering of the V. Lashkaryov Institute of Semiconductor Physics. His main research activities are physics of thin films, chromogenic materials and SIMS analysis, ion implantation, analysis of thin film and multilayer structures.
E-mail: s.kulbachynskyi@gmail.com,
https://orcid.org/0000-0001-6657-5569

Oleksandr Dubikovskyi, PhD in Physics and Mathematics, Researcher at the Department of Ion-Beam Engineering of the V. Lashkaryov Institute of Semiconductor Physics. He is the author of more than 16 publications. The main directions of his scientific activity are ion-beam modification and mass-spectrometry of semiconductor structures. E-mail: dubikovsky_o@ukr.net,
https://orcid.org/0000-0002-1504-8440

Authors' contributions

Efremov A.A.: data analysis, programming, modeling, writing – original draft, writing – review and editing.
Romanyuk B.M.: data analysis, writing – original draft.
Melnik V.P.: methodology, writing – review and editing.
Stadnik O.A.: investigation, methodology.
Sabov T.M.: conceptualization, supervision, writing – review and editing.
Kulbachynskyi O.A.: investigation, resources, data analysis, writing – original draft.
Dubikovskyi O.V.: methodology, writing – review and editing.

Дослідження природи фрактальності в плівках VO_2 та її впливу на фазовий перехід метал-ізолятор

А.А. Єфремов, Б.М. Романюк, В.П. Мельник, О.А. Стадник, Т.М. Сабов, О.А. Кульбачинський, О.В. Дубіковський

Анотація. Обговорено механізми, які лежать в основі виникнення фрактальної форми включень нової фази у плівках VO_2 під час фазового переходу метал-ізолятор. Отримані результати показують, що гістерезис температурної залежності опору $R(T)$ суттєво залежить від морфології та текстури плівки. Окрім цього спостерігаються деякі фрактальні особливості. Для визначення фрактальної розмірності D структурних елементів досліджуваних плівок за їхніми зображеннями було попередньо порівняно й обговорено різні підходи до фрактального аналізу. В результаті обробки зображень плівок було встановлено, що межі структурних елементів мають фрактальну розмірність від 1.3 до 1.5 і вище та корелюють з формою $R(T)$. Фрактальні межі вказують на домінуючу роль пружних напружень у фазовому переході плівок, що підтверджено чисельним моделюванням. На основі цих результатів запропоновано аналітичну модель, яка пов'язує вільну енергію плівки з фрактальною розмірністю її складових. Залежно від співвідношення пружної та міжфазної питомих енергій положення мінімуму вільної енергії F відповідає певній фрактальній розмірності D. Малі значення міжфазної енергії приводять до більшої фрактальної розмірності, що робить початкову фазу більш стабільною. Цей висновок добре пояснює всі ефекти, що спостерігаються експериментально у VO_2. Отримані результати дають змогу краще зрозуміти вплив структури і морфології на інші властивості досліджуваних плівок.

Ключові слова: фазовий перехід метал-ізолятор, VO_2 плівки, чисельне моделювання.